Journal of Alloys and Compounds 509 (2011) 6206–6211

Contents lists available at ScienceDirect

Journal of Alloys and Compounds

journal homepage: www.elsevier.com/locate/jallcom

One-step synthesis of MFe_2O_4 (M = Fe, Co) hollow spheres by template-free solvothermal method

Wangchang Li [a], Xiaojing Qiao [a,*], Qiuyu Zheng [b], Tonglai Zhang [a]

[a] State Key Laboratory of Explosion Science and Technology, Beijing Institute of Technology, Beijing 100081, PR China
[b] School of Civil Aviation and Safety Engineering, Shenyang Aerospace University, Shenyang 110136, PR China

ARTICLE INFO

Article history:
Received 23 November 2010
Received in revised form 24 February 2011
Accepted 25 February 2011
Available online 5 March 2011

Keywords:
Solvothermal
Magnetism
Hollow spheres
Ferrites

ABSTRACT

Monodispersed magnetic MFe_2O_4 (M = Fe, Co) hollow spheres were synthesized by simple template free solvothermal method in ethylene glycol (EG) solution. The hollow spheres were in the same size with an average diameter of about 360 nm and the shells of these spheres were about 80 nm, consisted of closely packed nanocrystallines due to Ostwald ripening. EG plays the key role in the synthesis of hollow spheres in contrast with octahedral crystals synthesized in aqueous solution. The products synthesized in aqueous solution were calcined at 800 °C and 1000 °C. The amount of spinel ferrite products increased monotonically with the increase of temperature and appeared as a single phase at 1000 °C. The saturation magnetization (M_s), remanent magnetization (M_r) and coercivity (H_c) for Fe_3O_4 hollow spheres was 74.47 emu/g, 2.59 emu/g and 32.503 Oe respectively whereas the reading of the same indicators for $CoFe_2O_4$ hollow spheres was 69.07 emu/g, 14.46 emu/g and 242.79 Oe, respectively. The magnetic variation between Fe_3O_4 and $CoFe_2O_4$ hollow spheres was caused by the radius difference of Fe^{2+} ($3d^6$) and Co^{2+} ($3d^7$) ions and it was also relevant with nanocrystal sizes of the spin disorder of crystal surface.

1. Introduction

In recent years, hollow structure nanoparticles have evoked immense interest of numerous researchers due to their unique physical and chemical properties, such as having a large specific surface area and low density which greatly exhibit potential applications in optics [1–3], photonic catalysis [4,5], fuel cells [6], lithium ion batteries [7], medicine release [8,9] and targeted drug delivery [10]. Many methods have been developed for preparing the hollow spheres. For instance, composite spheres, oxide and hollow polymer with diameters at the micron level can be produced by aerosol route [11], chemical vapor deposition [12], microwave assisted synthesis [13], ultrasound [14] etc. However, the main process for the preparation of hollow spheres generally requires removable templates such as monodispersed silica, polystyrene latex spheres, metal nanoparticles, gas bubbles and polymer spheres followed by sequential adsorption of magnetic nanoparticles on the templates [15–22]. The typical procedure is that the template is coated by either direct surface reaction utilizing special functional groups on the core or controlled precipitation of inorganic precursors on the surface of template to induce coating, followed by the removal of template core through calcination or solvent dissolution [23–25].

Definitely, there are many disadvantages of above mentioned methodologies and then the template-free methods have drawn increasing attentions. Mazloumi et al. [26] prepared nanostructure hollow microspheres through self-assembly of ZnO nanoparticles by a moderate template-free hydrothermal route in a mixture of ethanol (C_2H_5OH) and triethanolamine (TEA, $C_6H_{15}NO_3$). Chen et al. [27] prepared $NiFe_2O_4$ hollow nanospheres with diameter in the range of 90–180 nm via direct hydrothermal decomposition of a gel of Ni–Fe–EG (EG = ethylene glycol) in water solution. Chen and co-workers [28] reported the synthesis of $CoFe_2O_4$ hollow spheres with size ranging from 600 nm to 1 μm through hydrothermal treatment of an aqueous solution containing glucose, ammonium iron(II) sulfate hexahydrate [$(NH_4)_2Fe(SO_4)_2{\cdot}6H_2O$] and cobalt(II) sulfate heptahydrate [$CoSO_4{\cdot}7H_2O$], followed by calcination.

The purpose of our study is to synthesize monodispersed purified hollow ferrite spheres in low temperature from EG solution with simple template free solvothermal method. Cobalt chloride and ferric chloride were used as cation sources in the reaction system. EG and PVP were used as solvent and surfactant respectively. The diameter of prepared hollow spheres was in the range of 340–390 nm with narrow size distribution.

2. Experimental

2.1. Sample preparation

All chemicals were of analytical grade and purchased from Sinopharm Chemical Reagent Co., Ltd. without further purification. The starting materials for the

* Corresponding author. Tel.: +86 10 68912448; fax: +86 10 68912448.
E-mail address: XiaojingQiaobit@163.com (X. Qiao).

0925-8388/$ – see front matter.
doi:10.1016/j.jallcom.2011.02.157

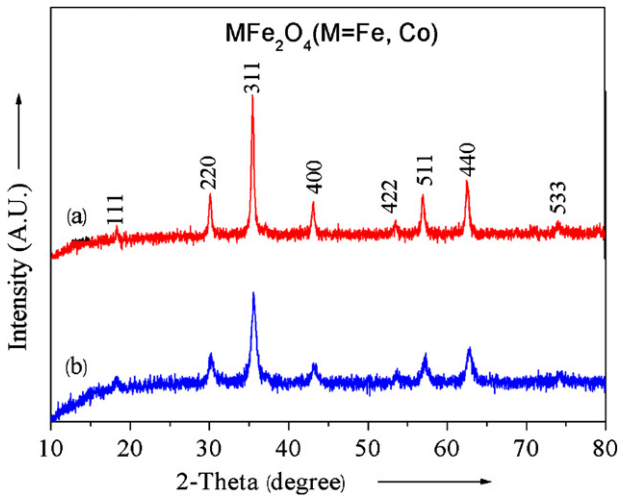

Fig. 1. XRD patterns of Fe_3O_4 (a) and $CoFe_2O_4$ (b) synthesized in EG solution.

present study included: $FeCl_3{\cdot}6H_2O$, $CoCl_2{\cdot}6H_2O$, urea, EG and polyvinylpyrrolidone (PVP).

A typical synthesis was performed as follows: 10.81 g $FeCl_3{\cdot}6H_2O$ and 4.76 g $CoCl_2{\cdot}6H_2O$ were dissolved into 80 mL EG. About 5 g urea and 0.4 g PVP were added into the solution and stirred under room temperature to form a homogeneous brown solution. The solvothermal synthesis was carried out in a 100 mL Teflon-lined stainless-steel autoclave cell without any agitation for 20 h at 180 °C. The resultant particles were washed by alcohol carefully, filtered and then dried at 60 °C overnight.

$CoFe_2O_4$ hollow spheres were synthesized as above-mentioned route while Fe_3O_4 hollow spheres were prepared without $CoCl_2{\cdot}6H_2O$ added.

2.2. Sample characterization

The X-ray diffraction (XRD) analysis of prepared and milled samples was carried out by using a Rigaku D/max-2500 X-ray diffractometer with Cu $K\alpha$ radiation ($\lambda = 0.154178$ nm). The average grain size was determined from the full-width at half maximum (FWHM) of the (200), (311), (400), (511) and (440) reflection of the XRD patterns by using Scherrer's formula. IR transmittance spectra of these hollow ferrite powder samples were measured on Bruker Equinox 55 infrared spectrophotometer (KBr pellets) in the range of 4000–400 cm^{-1}. Surface morphological features of the prepared and milled samples were observed by using a field emission scanning electron microscope (FESEM, S-4700, Hitachi, Japan) which operated at an accelerating voltage of 15 kV as well as Hitachi H-7500 (Hitachi, Japan) transmission electron microscopy (TEM) operated at 160 kV. Magnetic studies were carried out by using a HH-15 vibrating sample magnetometer (VSM) with fields up to 12000 Oe at room temperature.

3. Result and discussion

3.1. X-ray diffraction analysis

X-ray diffraction (XRD) patterns of all samples show very broad peaks, which indicating poor crystallinity and ultra-fine nature of the particles. XRD patterns of samples Fe_3O_4 and $CoFe_2O_4$ hollow spheres are shown in Fig. 1(a) and (b). All the samples perfectly match with the cubic spinel structure of Fe_3O_4 (JCPD card no. 88-0866) and $CoFe_2O_4$ (JCPD card no. 19-0629) with no extra peak observed. To calculate the crystallite size, a slow scan of selected diffraction peaks (200), (311), (400), (511) and (440) were recorded. From the full width at half maximum (FWHM) of peaks, the crystallite size was calculated by using the Scherrer's formula ($D = K\lambda/\beta\cos\theta$, $K = 0.89 = \lambda = 0.154178$ nm). All the structural parameters calculated from the peaks are listed in Table 1.

The diffraction peaks of $CoFe_2O_4$ crystallite are found broader than that of Fe_3O_4 as shown in Fig. 1. Most crystal faces of the $CoFe_2O_4$ crystallite possess smaller d values excluding (400) face if compared to Fe_3O_4 crystallite. Due to greater crystallite size and d values of Fe_3O_4, it is also concluded that the Fe_3O_4 crystallite grows faster than $CoFe_2O_4$ crystallite. Lattice parameter, $a = 8.392$ Å for $CoFe_2O_4$ and $a = 8.385$ Å for Fe_3O_4 was calculated. This was attributed to the differences in ionic radii of Co^{2+} (0.78 Å) and Fe^{2+} (0.65 Å).

The X-ray density or theoretical density was estimated by using the relation [29],

$$\text{X} - \text{ray density } (D_X) = \sum \frac{A}{N \times V} \quad (1)$$

Where, A is the sum of atomic weights of all atoms in the unit cell, V is volume of the unit cell and N is the Avogadro's constant.

Since each primitive unit cell of the spinel structure contains eight molecules, the X-ray density of ferrites, "$D_{ferrite}$" was determined by using the following relation [30]:

$$\text{X-ray density } (D_{ferrite}) = \frac{8M}{N \times a^3} \quad (2)$$

where, M is the molecular weight of particular ferrite, N is the Avogadro's constant and a^3 is the volume of cubic unit cell. In fact, apparent densities are much lower than the X-ray densities due to the hollow spherical structure.

3.2. FTIR spectroscopic characterization

Theoretically, all AB_2O_4 types of normal and inverse spinel oxides of transition metals have four infrared active modes. These vibrations occur in the ν_1 (650–550 cm^{-1}), ν_2 (525–390 cm^{-1}), ν_3 (380–335 cm^{-1}) and ν_4 (300–200 cm^{-1}) regions [31].

The ν_1 and ν_2 bands are generated owing to intrinsic vibrations of tetrahedral and octahedral coordination compounds. Absorption of ν_1 is caused by the bond stretching of tetrahedral metal ions and oxygen, while ν_2 vibration is observed due to the vibration of oxygen in the direction perpendicular to the axis joining the tetrahedral ions and oxygen; The ν_3 mode is obtained from the Fe^{3+}–O complexes at octahedral sites [32]. The frequency of ν_4 vibration depends on the mass of tetrahedral metal ion complexes, which gives information about the vibration of ions occupying at tetrahedral site.

IR spectrum recorded at 620 and 462 cm^{-1} as shown in Fig. 2(a) indicates characteristic peaks of tetrahedral and octahedral Fe–O stretching for Fe_3O_4 while 590 and 443 cm^{-1} for $CoFe_2O_4$ as shown in Fig. 2(b). The values of the force constant K_T and K_O for the T_d and O_h sites were 279.33 dyn/cm and 155.10 dyn/cm for Fe_3O_4, whereas for $CoFe_2O_4$ the readings were 252.83 dyn/cm and 142.54 dyn/cm calculated according to the following relation [33].

$$K = 4\pi^2 c^2 \nu^2 m \quad (3)$$

Table 1
Structural parameters of Fe_3O_4 and $CoFe_2O_4$ crystallite.

Samples	d (nm)					Crystallite size (nm)	Lattice parameter 'a' (Å)	X-ray density (g/cm^3)
	(200)	(311)	(400)	(511)	(440)			
Fe_3O_4	2.9625	2.5254	2.0927	1.6130	1.4811	28.32	8.385	5.23
$CoFe_2O_4$	2.9491	2.5114	2.0992	1.6097	1.4793	13.4	8.392	5.28

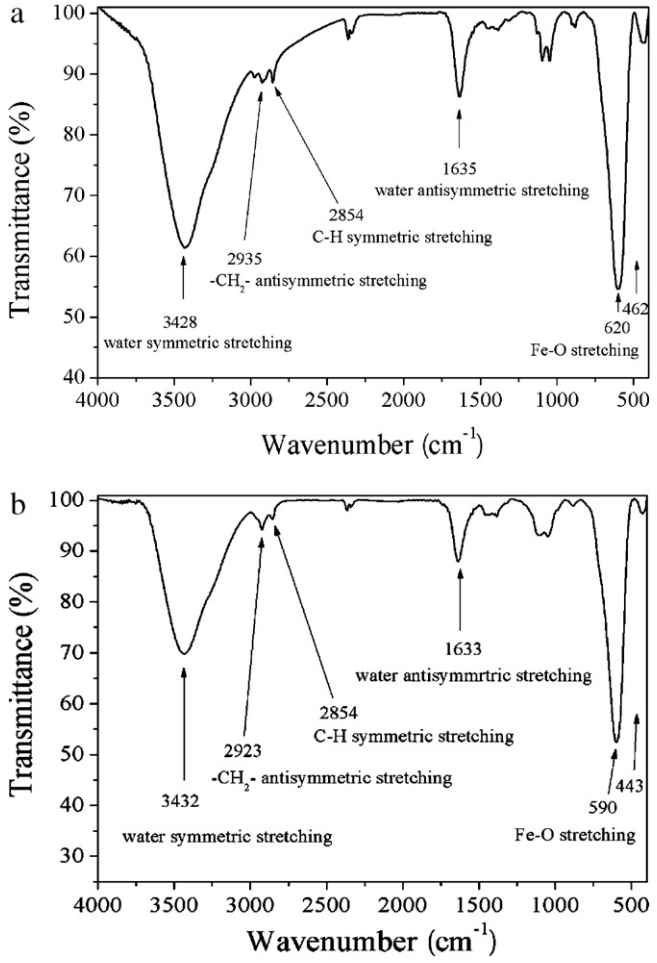

Fig. 2. IR spectrum of Fe_3O_4 (a) and $CoFe_2O_4$ (b) hollow spheres synthesized in EG solution.

where, ν is the vibration frequency of T_d and O_h. c is the speed of light 2.99×10^8 m/s. m is the reduced mass for Fe^{3+} ions and the O^{2-} ions (2.06×10^{23} g).

In addition to these vibrational modes, a broad hump due to antisymmetric stretching of –OH with maxima at about 3428 cm^{-1} and bending mode at 1635 cm^{-1} are observed in the spectrum. The broadness of stretching mode is attributed to the existence of EG absorbed on the surface of hollow spheres. Weak bands of C–H symmetric stretching and antisymmetric stretching of $–CH_2–$ groups are recorded at 2854 and 2935 cm^{-1}. The appearance of these peaks in the spectrum confirmed the presence of PVP and adsorbed EG on the surface of particles.

3.3. TEM analysis

Fig. 3 reveals the TEM images of Fe_3O_4 (a) and $CoFe_2O_4$ (b) hollow spheres. Uniform hollow spheres with monodispersed are observed in the low-magnification TEM image. It is clear that the obtained samples are hollow structure and approximately in the same size with an average diameter of about 360 nm. The surface of the spheres shows a protrusive nanostructure with average size of about 80 nm for Fe_3O_4 hollow spheres and 85 nm for $CoFe_2O_4$ hollow spheres observed in the high-magnification TEM image. The shells of the hollow spheres are packed with nanocrystallines revealing imperfect spherical morphology. According to TEM investigations, it can be concluded average diameter of nanocrystallines are in range of 10–30 nm which is to some extent close to the average crystallite size calculated through XRD analysis.

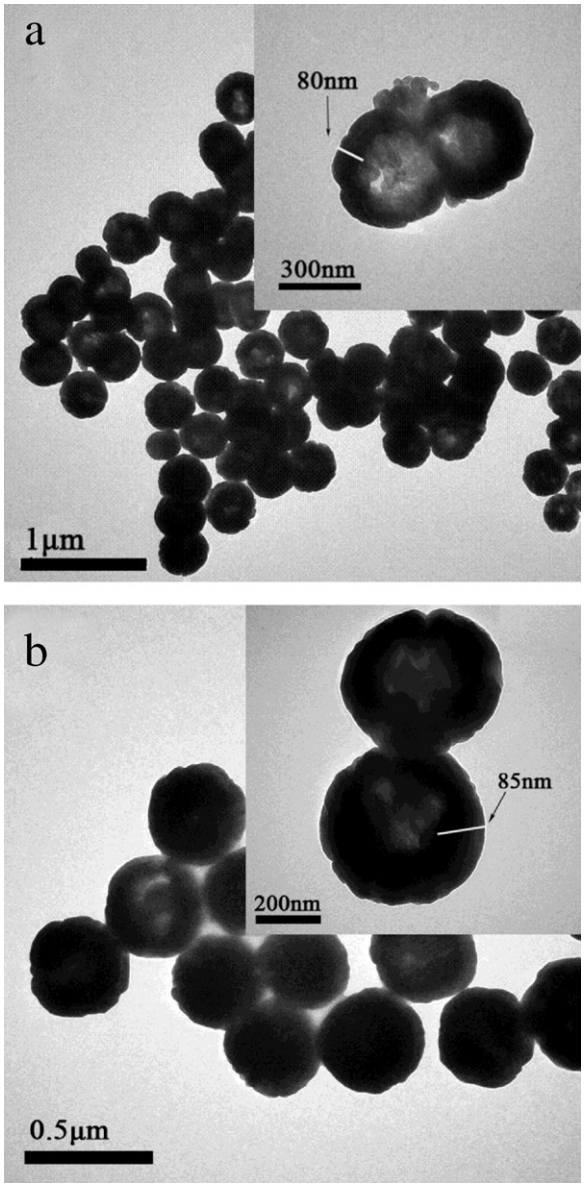

Fig. 3. TEM images of Fe_3O_4 (a) and $CoFe_2O_4$ (b) hollow spheres synthesized in EG solution.

3.4. FESEM analysis

The morphologies of the hollow sphere products were also investigated by FESEM measurement (Fig. 4). Most of the particles are observed to be fully spherical. It can be seen that the diameter of the hollow spheres are in the range of 340–390 nm with average size of 360 nm in correspondence with the TEM images. The shells of hollow ferrite spheres are consisted of closely packed nanocrystallines with the size of 10–30 nm.

3.5. Solvent and PVP effects

EG plays the key role in the synthesis of hollow spheres. The ferrites were also synthesized in aqueous solution to explore the effect of EG in the formation of hollow spheres. The method was the same with preparation of hollow spheres except the substitution of EG by water as solution. Fig. 5 indicates the size and morphology of

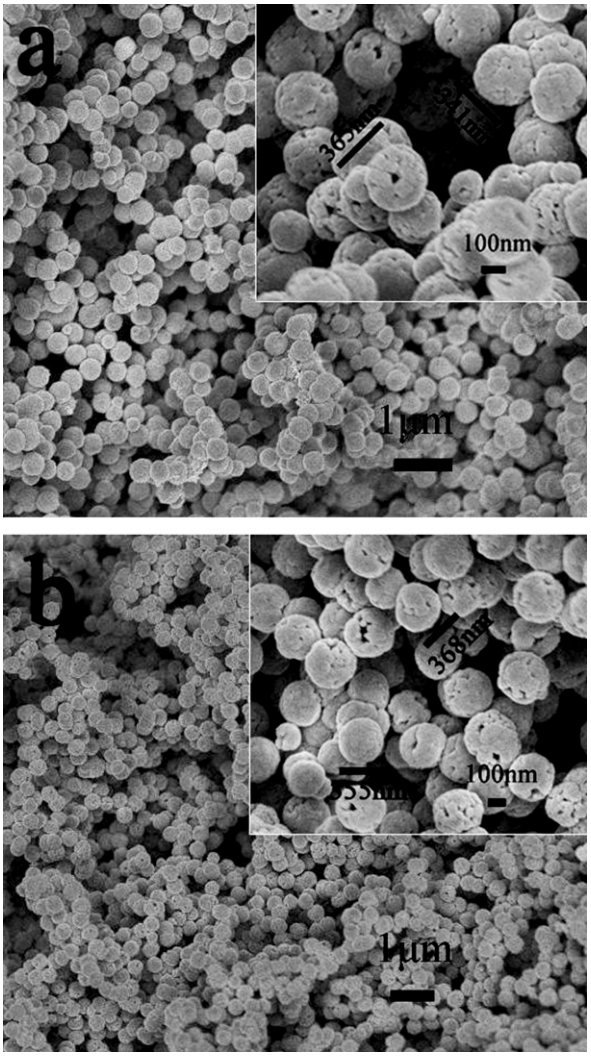

Fig. 4. FESEM images of Fe_3O_4 (a) and $CoFe_2O_4$ (b) hollow spheres synthesized in EG solution.

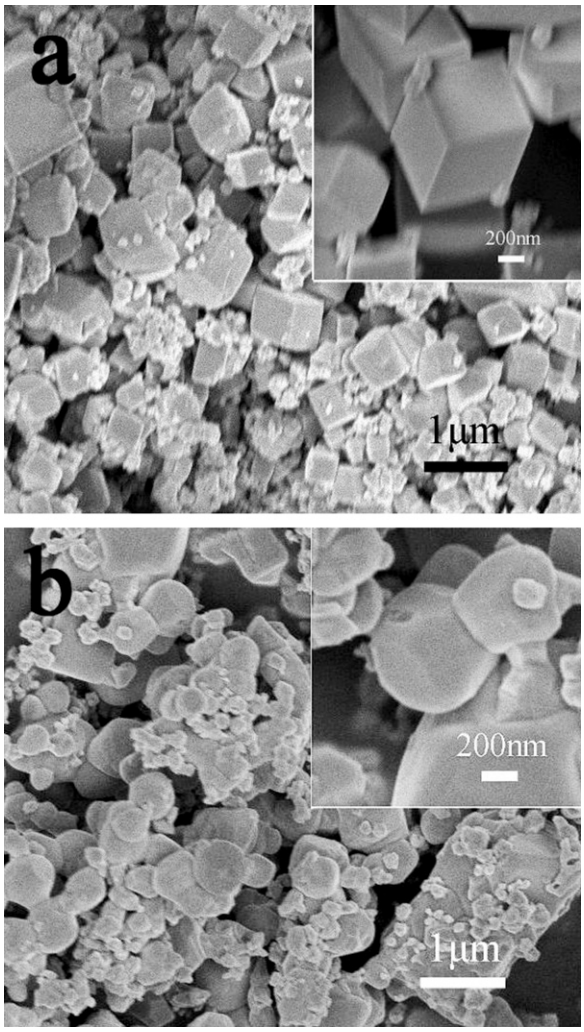

Fig. 5. FESEM images of $CoFe_2O_4$ synthesized in water solution: (a) precursor and (b) $CoFe_2O_4$ calcined at 1000 °C for 2 h.

ferrite reacted in the water solution. In comparison with Figs. Fig. 4 and 5(a) shows that the octahedral crystals were completely different from the hollow spheres though some crystals with irregular shapes were also obtained.

PVP affects the morphology and size of the aggregated particles especially in the refinement of crystals. At first, PVP may arise in the steric effect due to its long polyvinyl chain and prevent the particles from aggregation when PVP was being absorbed on the surface of MFe_2O_4 particles. Second, relative surface free energies of the MFe_2O_4 crystal facets are changed because of PVP absorbed on the crystal facets. It is also potential to block sites which are essential to the incorporation of new growth units into the crystal lattice. Consequently, these two effects may change the crystal growth kinetics and then influence on the size and morphology of the particles.

In the present work, inorganic–organic hybrid Fe–Co–EG complex was formed in the starting solution. As the temperature and pressure increased in the solvothermal route, OH^- was released gradually for urea decomposition and at the same time Fe^{3+}/Co^{2+} was dissociated from Fe–Co–EG complex for EG evaporation. Then the process of ferrite crystal nucleation took place as per Eq. (4). PVP as surfactant absorbed on the surface of crystal nucleation restrained the growth of crystal nucleus. With the reaction continued, the hollow structure was formed gradually due to the self-assembly of nanocrystals. Meanwhile, the Fe–Co–EG complex would not form in the aqueous solution and the reaction of Eq. (4) happened directly in appropriate temperature and pressure. Hence, the octahedral crystals were synthesized and grew rapidly in aqueous solution as revealed in Fig. 5(a).

$$2Fe^{3+} + Co^{2+} + 8OH^- \xrightarrow{\text{Solvothermal}} CoFe_2O_4 + 4H_2O \quad (4)$$

The FESEM analysis was supplemented by XRD analysis to aid further interpretation of the reaction processes. Fig. 6 shows the XRD patterns of precursor and ferrite calcined at 800 °C and 1000 °C. The XRD pattern of the precursor indicates that Fe_2O_3 (JCPD card no. 39-0238) and $CoCO_3$ (JCPD card no. 11-0692) were present as major phases and $CoFe_2O_4$ (JCPD card no. 03-0864) existed as minor phase. It is noteworthy that the presence of some weak peaks relating to $CoFe_2O_4$ in precursor diffractogram implies high thermal energy was produced during the hydrothermal reaction. However, unlike the reaction in EG, the single phase spinel ferrites was not synthesized directly in aqueous solution. It was formed gradually from some intermediate phases due to its complicated crystalline structure. The interaction between highly reactive Co^{2+} ions and CO_2 in the air has led to the formation of $CoCO_3$ during the drying process. When the calcination temperature was increased to 800 °C, $CoCO_3$ decomposed and liberated Co^{2+} reacted with Fe_2O_3 to form a small amount of ferrite $CoFe_2O_4$ as per Eq. (5). The amount of

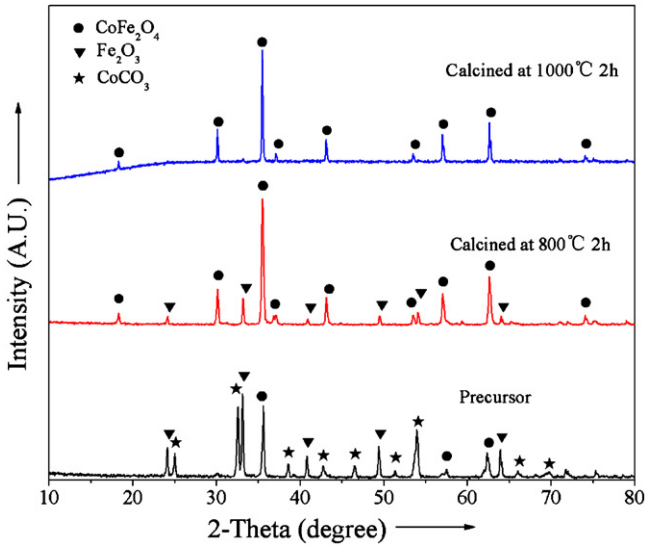

Fig. 6. XRD patterns of $CoFe_2O_4$ synthesized in water solution at various calcined temperature.

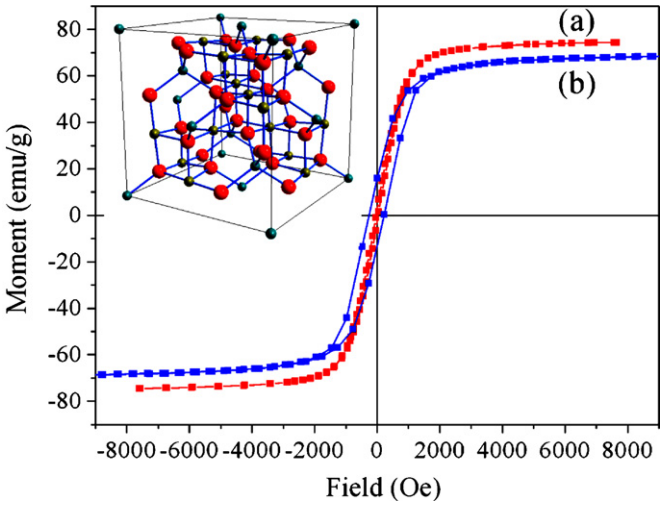

Fig. 7. Room temperature hysteresis loops for Fe_3O_4 (a) and $CoFe_2O_4$ (b) hollow spheres.

$CoFe_2O_4$ increased monotonically with the increase of temperature and appeared as a single phase at 1000 °C.

$$Fe_2O_3 + CoO \overset{800-1000^{\circ}C}{\longrightarrow} CoFe_2O_4 \quad (5)$$

3.6. Magnetization measurement

VSM results (Fig. 7) show the saturation magnetization (M_s), remanent magnetization (M_r), and coercivity (H_c) values of Fe_3O_4 and $CoFe_2O_4$ hollow spheres were 74.47 emu/g and 69.07 emu/g, 2.59 emu/g and 14.46 emu/g as well as 32.503 Oe and 242.79 Oe respectively. The size and morphology of Fe_3O_4 and $CoFe_2O_4$ hollow spheres were similar while the VSM results show very distinct characteristics. These plots show that the saturation magnetization and remanent magnetization of $CoFe_2O_4$ were lower than those of Fe_3O_4 while coercivity was much higher than Fe_3O_4, which may be due to the substitution of Fe^{2+} ions by Co^{2+} ions on the octahedral sites.

Ferrimagnetism happens in spinel structure ferrite due to double exchange mechanism. In addition, the level of double exchange mechanism depends on the degree of overlap of electron orbits. Spinel structure ferrite contains an equal mixture of Fe^{2+} (Co^{2+}) and Fe^{3+} ions on octahedral sites, together with the same number of Fe^{3+} ions on tetrahedral sites. A double exchange interaction ferromagnetically aligns the Fe^{2+} (Co^{2+}) and Fe^{3+} ions on the octahedral sites. The Fe^{3+} ions on the tetrahedral sites do not participate in antiferromagnetic superexchange interaction. Thus the two sets of Fe^{3+} ions cancel out, leaving a net moment due to the Fe^{2+} ions alone.

The difference of magnetism between Fe_3O_4 and $CoFe_2O_4$ can be explained by Heisenberg Hamilton Function as follows [34]:

$$H = -2\sum_{i>j} J_{ij} S_i S_j \quad (6)$$

where, J_{ij} is the exchange integral between the spins situated at site i and j. S_i is the atomic spin of the magnetic ion located on i site. The factor "2" in Eq. (5) arises from the fact that, when summing over all possible pairs exchange interactions, we count each pair twice.

The exchange constant J_{ij} strongly depends on the angle of the M–O–M bond and radius of metal ions. Compared with the 0.65 Å the radius of Fe^{2+} ($3d^6$) ion, the radius of Co^{2+} ($3d^7$) ion is 0.78 Å.

The d orbits can distort and split into e_g and t_{2g} as the result of the Jahn–Teller effect. An extra electron in t_{2g} orbits and a higher degree of overlap between e_g electron orbits of Fe_3O_4 due to smaller radius of Fe^{2+} ($3d^6$) explained the reason of higher saturation magnetization of Fe_3O_4 compared to $CoFe_2O_4$. The far higher remanent magnetization and coercivity values of $CoFe_2O_4$ than Fe_3O_4 are also probably related to the difference of radius.

Besides, the crystalline size has also intensively affected the magnetism characteristics. From the XRD pattern, the crystalline sizes of Fe_3O_4 and $CoFe_2O_4$ were found to be 28.32 nm and 13.4 nm. Due to the decrease of the crystalline size, the spin disorder of the crystal surface increases which strengthens the Second-Order Tunneling effect. The saturation magnetization of Fe_3O_4 crystal is higher than that of $CoFe_2O_4$ crystal because more atom magnetic moment is in disordered state on $CoFe_2O_4$ crystal surface and this also makes the difference of coercivity values.

4. Conclusions

The monodispersed purified hollow ferrite spheres were successfully synthesized under low temperature through template free solvothermal method. The narrow size distributed 340–390 nm hollow spheres possessed 80 nm-wide shells which consisted of closely packed 10–30 nm sized nanocrystallines as a result of Ostwald ripening. EG plays key role in the synthesis of hollow spheres in contrast to octahedral crystals synthesized in the water solution. VSM results showed that the saturation magnetization (M_s), remanent magnetization (M_r) and coercivity (H_c) values of Fe_3O_4 and $CoFe_2O_4$ hollow spheres were 74.47 emu/g and 69.07 emu/g, 2.59 emu/g and 14.46 emu/g as well as 32.503 Oe and 242.79 Oe, respectively. The differences of magnetism between Fe_3O_4 and $CoFe_2O_4$ hollow spheres owes to the radius difference of Co^{2+} ($3d^7$) ion and Fe^{2+} ($3d^6$) ion according to Heisenberg Hamilton Function while the crystalline size variation has also caused the difference.

Acknowledgement

We are sincerely thankful to the State Key Laboratory of Explosion Science and Technology to support our research.

References

[1] X. Xu, S.A. Asher, J. Am. Chem. Soc. 126 (2004) 7940–7945.
[2] C.R. Li, M.Y. Cui, Q.T. Sun, W.J. Dong, Y.Y. Zheng, K. Tsukamoto, B.Y. Chen, W.H. Tang, J. Alloys Compd. 504 (2010) 498–502.

[3] H.L. Niu, Q. Min, Z.Y. Tao, J.M. Song, C.J. Mao, S.Y. Zhang, Q.W. Chen, J. Alloys Compd. 509 (2011) 744–747.
[4] X.W. Lou, L.A. Archer, Z.C. Yang, Adv. Mater. 20 (2008) 3987–4019.
[5] J. Huang, W.M. Chen, W. Zhao, Y.Q. Li, X.G. Li, C.P. Chen, J. Phys. Chem. C 113 (2009) 12067–12071.
[6] W.M. Guo, J. Liu, C. Jin, J. Alloys Compd. 504 (2010) L21–L24.
[7] X.F. Guan, L.P. Li, G.S. Li, Z.W. Fu, J. Zheng, T.J. Yan, J. Alloys Compd. 509 (2011) 3367–3374.
[8] L.B. Chen, F. Zhang, C.C. Wang, Small 5 (2009) 621–628.
[9] A.V. Reis, M.R. Guilherme, A.T. Paulino, E.C. Muniz, L.H.C. Mattoso, E.B. Tarnbourgi, Langmuir 25 (2009) 2473–2478.
[10] Y.F. Zhu, Y. Fang, S. Kaskel, J. Phys. Chem. C 114 (2010) 16382–16388.
[11] S. Gumen, B. Ebin, J. Alloys Compd. 492 (2010) 585–589.
[12] S.L. Wang, X. Jia, P. Jiang, H. Fang, W.H. Tang, J. Alloys Compd. 502 (2010) 118–122.
[13] L. Zhang, X.F. Cao, Y.L. Ma, X.T. Chen, Z.L. Xue, Cryst. Eng. Commun. 12 (2010) 207–210.
[14] W. Liu, L.X. Cao, G. Su, H.S. Liu, X.F. Wang, L. Zhang, Ultrason. Sonochem. 17 (2010) 669–764.
[15] S.B. Ni, S.M. Lin, Q.T. Pan, F. Yang, K. Huang, X.Y. Wang, D.Y. He, J. Alloys Compd. 478 (2009) 876–879.
[16] C.-R. Lin, C.-C. Wang, I.-H. Chen, J. Magn. Magn. Mater. 304 (2006) e34–e36.
[17] M. Tada, T. Kanemaru, T. Hara, T. Nakagawa, H. Handa, J. Magn. Magn. Mater. 321 (2009) 1414–1416.
[18] C.-R. Lin, C.-C. Wang, M.-H. Hsieh, S.-Z. Lu, Y.-J. Siao, IEEE Trans. Magnetics 10 (2009) 4257–4260.
[19] C.L. Yan, D.F. Xue, J. Alloys Compd. 431 (2007) 241–245.
[20] Y.M. Li, W.Y. Li, S.L. Chou, J. Chen, J. Alloys Compd. 456 (2008) 339–343.
[21] C. Wang, C. Xiangfeng, W. Mingmei, Sens. Actuators B 120 (2007) 508–513.
[22] H.T. Schmidt, A.E. Ostafin, Adv. Mater. 14 (2002) 532–535.
[23] S. Gao, H. Zhang, X. Wang, R. Deng, D. Sun, G. Zheng, J. Phys. Chem. B 110 (2006) 15847–15852.
[24] C. Yan, D. Xue, J. Phys. Chem. B 110 (2006) 7102–7106.
[25] H. Kou, J. Wang, Y. Pan, J. Guo, Mater. Chem. Phys. 99 (2006) 325–328.
[26] M. Mazloumi, S. Taghavi, H. Arami, S. Zanganeh, A. Kajbafvala, M.R. Shayegh, S.K. Sadrnezhaad, J. Alloys Compd. 468 (2009) 303–307.
[27] L. Chen, H. Dai, Y. Shen, J. Bai, J. Alloys Compd. 491 (2010) L33–L38.
[28] Y. Meng, D.R. Chen, X.L. Jiao, Eur. J. Inorg. Chem. 2008 (2008) 4019–4023.
[29] B.D. Cullity, Elements of X-ray Diffraction, second ed., Addison-Wesley Publishing Company, Inc, United States of America, 1978, p. 89.
[30] P.A. Shaikh, R.C. Kambale, A.V. Rao, Y.D. Kolekar, J. Alloys Compd. 492 (2010) 590–596.
[31] C. Julien, M. Massot, C. Perez-Vicente, Mater. Sci. Eng. B 75 (2000) 6–12.
[32] R.D. Waldron, Phys. Rev. 99 (1955) 1727–1735.
[33] S.A. Mazen, H.M. Zaki, S.F. Mansour, Int. J. Pure Appl. Phys. 3 (1) (2007) 40.
[34] R. Masroura, M. Hamedounc, A. Benyoussef, J. Alloys Compd. 503 (2010) 299–302.